PCCP

From weak to strong interactions: Structural and electron topology analysis of the continuum from the supramolecular chalcogen bonding to covalent bonds

Journal:	*Physical Chemistry Chemical Physics*
Manuscript ID	CP-ART-11-2021-005441.R2
Article Type:	Paper
Date Submitted by the Author:	03-Mar-2022
Complete List of Authors:	Miller, Daniel; Ball State University, Chemistry Chernyshov, Ivan; ITMO University, SCAMT Laboratory Torubaev, Yury; d. N.S. Kurnakov Institute of General and Inorganic Chemistry of the Russian Academy of Sciences Rosokha, Sergiy; Ball State University, Chemistry

ARTICLE

From weak to strong interactions: Structural and electron topology analysis of the of the continuum from the supramolecular chalcogen bonding to covalent bonds

Received 00th January 20xx,
Accepted 00th January 20xx

DOI: 10.1039/x0xx00000x

Daniel K. Miller,[a] Ivan Yu. Chernyshov;[b] Yury V. Torubaev,[c*] Sergiy V. Rosokha[a*]

Relation between covalent and supramolecular bonding, and the criteria of the assignments of different interactions were explored via the review of selenium and tellurium containing structures in the Cambridge Structural Database and their computational analysis using Quantum Theory of Atoms in Molecules (QTAIM). This combined study revealed continuums of the interatomic Se···Br and Te···I distances, $d_{Ch...X}$, in the series of associations from the sums of the van der Waals radii of these atoms ($r_{Ch} + r_X$) to their covalent bond lengths. The electron densities, $\rho(r)$, at Bond Critical Points (BCPs) along the chalcogen bond paths increased gradually from about 0.01 a.u. common for the non-covalent interactions to about 0.1 a.u. typical for the covalent bonds). The log $\rho(r)$ values fell on the same linear trend line when plotted against normalized interatomic distances, $R_{XY} = d_{Ch...X}/(r_{Ch} + r_X)$. The transition from the positive to negative values of the energy densities, H(r), at the BCPs (related to a changeover of essentially non-covalent into partially covalent interactions) were observed at $R_{XY} \approx$ 0.80. Synchronous changes of bonding characteristics with R_{XY} (similar to that found earlier in the halogen-bonded systems) designated normalized interatomic separation as a critical factor determining nature of these bondings. The uninterrupted continuums of Te···I and Se···Br bond lengths and BCPs' characteristics signified an intrinsic link between limiting types of bonding involving chalcogen atoms and between covalent and supramolecular bondings in general.

Introduction

Following a recognition of ubiquity of halogen bonding (HaB) and its high potential for crystal engineering, catalysis and other applications, the attention of the chemical community turned to its sister supramolecular interactions involving chalcogen, pnicogen and tetrel atoms.[1-5] As a result, just six years after HaB was defined by IUPAC in 2013,[6] chalcogen bonding (ChB) was officially acknowledged as a "net attractive interaction between an electrophilic region associated with a chalcogen atom in a molecular entity and a nucleophilic region in another, or the same, molecular entity".[7]

The analogous definitions underscore similarity of these supramolecular interactions and also the difficulty in separation of some phenomenon out of the complex and continuous background.[§] Indeed, one of us has noted recently that ChB is not a stand-alone type of bonding and a smooth transition from covalent to hypervalent (3c-4e) bonding and further to non-covalent interactions may be observed for heavy chalcogens like Se and Te.[8†] This concept of ChB as a part of the covalent to noncovalent interaction (NCI) continuum is consistent with the earlier studies of the covalent bonds / NCI continuum for N···Br bonding in the series of complexes of bromine-containing electrophiles with 1,4-diazabicyclo[2.2.2]-octane[9] (and in more recent study of similar HaB associations with halide anions[10]). Comparable smooth transition from the ligand-to-metal coordinative bond to the metal-to ligand HaB was found in the associations involving Cu, Ag, Au, Pt or Hg metals as HaB acceptors.[11] Analogous variations were also noted for the MF_4-base interactions[12] and for tetrel-bonded complexes.[13] The idea of ChB as a part of a larger continuum is also consistent (at the long-distance end) with the concept of the supramolecular interactions as the expanded case of 3c- 4e bonding.[14-16] In fact, it was noted that the X-Ch-X three-body systems "*show a continuous variation of the distances of the two Ch-X bonds ··· without indications of critical distances at which the bonds switch from the substantially covalent to the predominantly electrostatic nature*".[16] Another important observation of "*continuous distribution of distances*" for Te···O contacts which "*prevents us from establishing a sharp borderline between bonded and non-bonded interactions based on a distance criterion*" was made by Alvarez.[17] A similar conclusion was made regarding the energies of intermolecular interactions in tellurium compounds which "*may approach that of a hypervalent single bond*".[18,19] This suggests the applicability of the HOMO-LUMO model for the analysis of intermolecular interaction in the HaB and ChB systems, where the Ch···X distances formally exceed those for the valent and hypervalent interactions.[20-23]

[a] *Chemistry Department, Ball State University, Muncie, IN, 47306, USA.*
[b] *TheoMat group, ChemBio Cluster, ITMO University, Lomonosova 9, St. Petersburg, 191002, Russia*
[c] *N.S. Kurnakov Institute of General and Inorganic Chemistry, Russian Academy of Sciences, GSP-1, L eninsky prospect, 31, Moscow, 119991, Russia.*

Electronic Supplementary Information (ESI) available: Distributions of geometric characteristics of Ch-X contacts (Ch = , X =), structures selected for QTAIM analysis, dependencies of potential and kinetic energy densities at BCPs, experimental and calculated interatomic separations, topological characteristic of BCPs, energies oand coordinates of the associations. See DOI: 10.1039/x0xx00000x

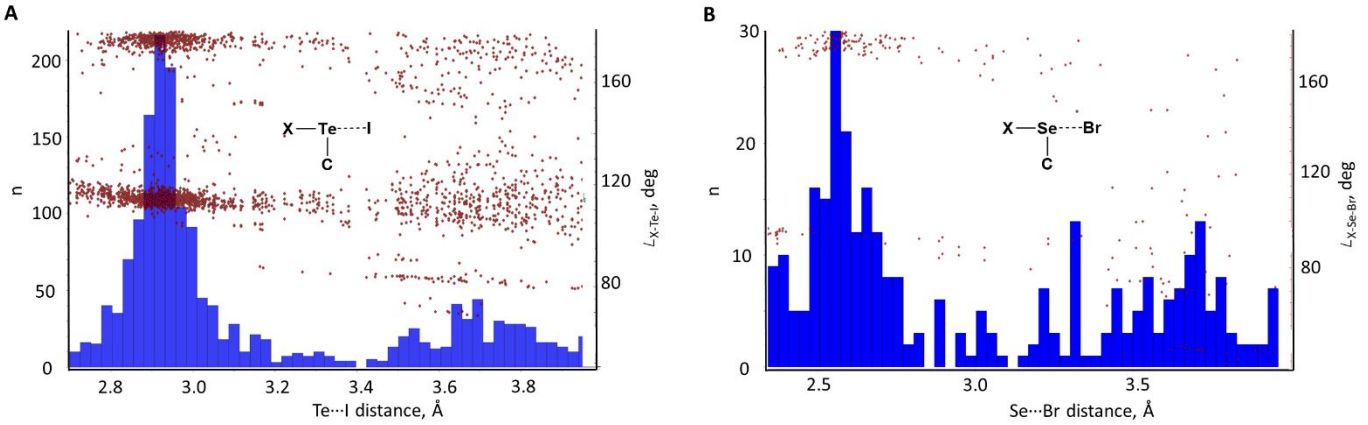

Figure 1. Distance and angles distribution in the Ch···Hal contacts (blue columns, left axes, A: Ch = Te, Hal = I, B: Ch = Se, Hal = Br) and the scattering of the X···Ch···Hal angles (red dots, right axes) with the Ch···Hal distance (X = any atom).

While the publications cited above pointed out the wide variations of the energies and bond lengths involving chalcogen atoms, systematic studies of the transition from supramolecular to covalent bonding in such systems and the accompanying changes in the nature and properties of these interactions with the decrease of the interatomic distances are lacking. As such, in the current work we present the results of the analysis Cambridge Structural Database (CSD)[24,25] of the chalcogens-containing contacts together with the scrutiny of the transformation of these interactions using Bader's Quantum Theory of Atoms in Molecules (QTAIM).[26-28] Previous applications of QTAIM to the series of hydrogen-bonded (HyB) and HaB complexes demonstrated continuous variations of the characteristics of these bond critical points (BCPs) with a decrease of the interatomic distances from the van der Waals separations to the covalent bonds.[28-32] Based on the topology of electron densities and energies at BCPs, the interactions in these systems were classified as non-covalent (closed-shell), covalent (shared-shell) and intermediate (partially-covalent) bonding.[29,31] Moreover, synchronous changes of the bonding characteristics with the normalized interatomic separations, $R_{XY} = d_{XY}/(R_X + R_Y)$ (where d_{XY} is an interatomic X-Y distance, and R_X and R_Y are van der Waals radii of X and Y) in the HaB systems suggested the R_{XY} could be used for the classification of the interactions.[31] In the current work we examine changes in the topologies of the electron densities and energies, and therefore nature of bonding, with the interatomic distances in the ChB systems. For clarity, the scope of the current study is limited to the structures containing Te-I and Se-Br interactions.[$$] These structures provided abundant examples of the diverse representative systems showing diagonal similarity**.**

The question about the distance criterion in chalcogen bonding,[16,33] and a vital role of normalized separations in the HaB systems[31] draws special attention to the values of the van der Waals radii of the interacting atoms. Indeed, while the majority of the studies of intermolecular interactions rely onto the radii listed in the seminal publication of Bondi,[34] a number of subsequent studies suggested alternative methodologies leading to somewhat different (especially for the heavier atoms) values.[33, 35-36] In particular, the revised values of the van der Waals radii were established recently for many atoms (including bromine, selenium and iodine relevant for the current work) using line-of-sight (LoS) approach.[38] In this method, evaluation of the van der Waals radii is based on the interatomic contacts which are almost free from the "shielded" effects of the neighboring atoms or groups, and, thus, they depend on the intrinsic properties of the interacting entities. Therefore, in the context of the analysis of the continuum for Ch···Hal bonding, we also re-evaluated the van der Waals for tellurium using LoS approach.

Results and discussion

1. CSD analysis of the structurtal features of the Te···I and Se···Br contacts.

In order to elucidate wide-range variations of the characteristics of Te···I and Se···Br interactions, we started with the survey of their structural features. The structures containing Te···I and Se···Br covalent bonds and non-covalent contacts were extracted from the CSD.[25] The combined data (arranged as the distance distribution histograms of the corresponding contacts together with the corresponding ·X···Ch···Hal angles) are presented in Figure 1. Relationships between variations of C-Ch···Hal angles vs Ch···Hal distances or X-Ch···Hal angles are shown in Figures S1 and S2 in the ESI.

A glance at the diagrams in Figure 1 reveals that the database contains much more Te···I than Se···Br contacts. In each of these series, the points are grouped around two favorable separations. Specifically, the Te···I contacts are found mostly around about 2.9 Å and 3.7 Å, and Se···Br contacts are clustered around 2.6 Å and 3.6 Å distances. It is noticeable, however, that these distributions are broad and there are many points between the maxima which eliminate any large gaps between successive entries. As such, both series comprise points covering whole range of the interatomic distances, from about 2.7 Å to 4.0 Å in case of the Te···I systems, and from about 2.3 Å to 3.9 Å for the Se···Br contacts. Similar continuums of the interatomic distances were found in distributions of Te···Br, Te···Cl, Te···O, and Se···Cl contacts (Figures S3-S6 in the ESI). These diagrams confirm the continuum of Ch···X bond lengths, which show a gradual increase from the covalent bonds to van der Waals separations in a series of chalcogen-containing structures.

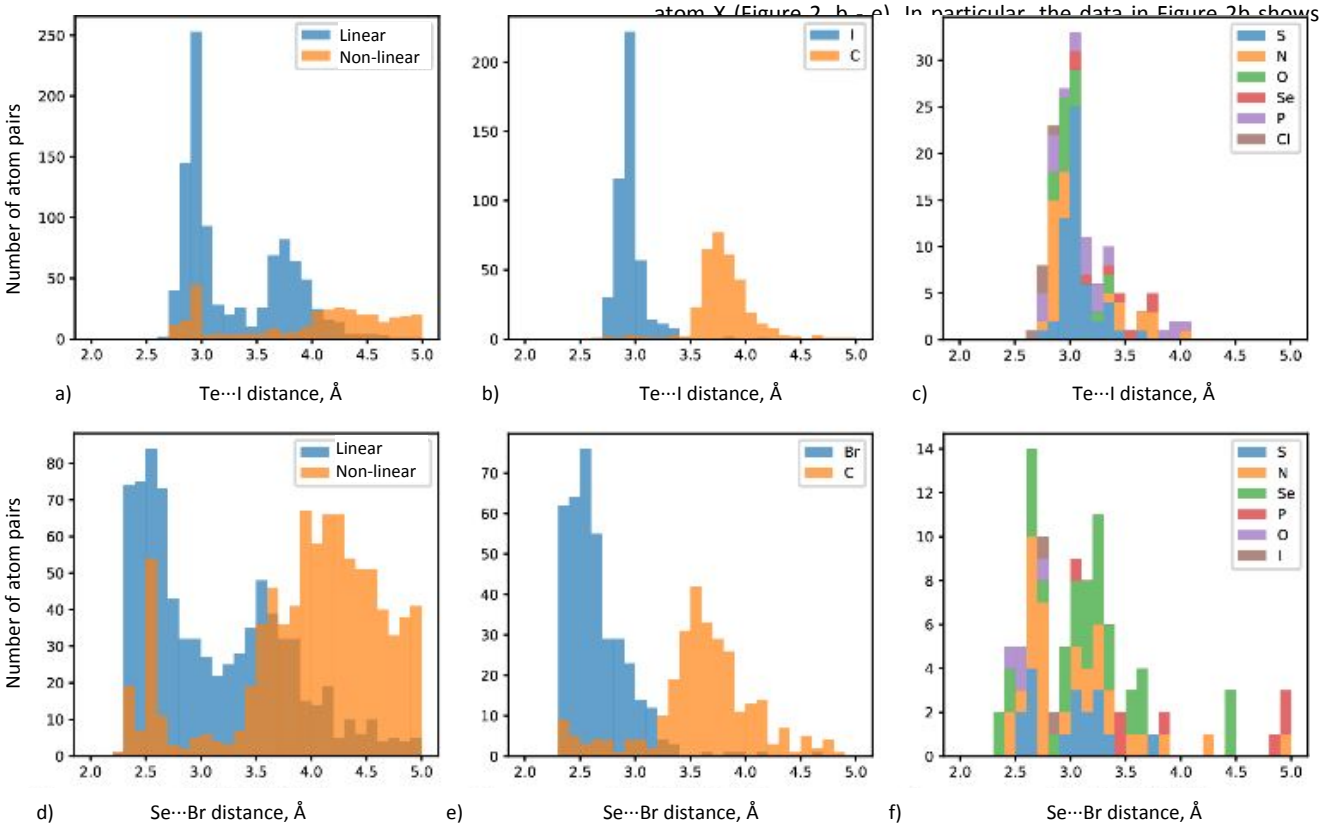

Figure 2. Distance distributions of linear and non-linear X-Te···I (a) and X-Se···Br (d) interactions, linear C/I–Te···I (b) and C/I–Se···Br (e) contacts, and other linear X–Te···I (c) and X–Se···Br (f) contacts. Legends of (b), (c), (e), and (f) panels denote element X in X–Te···I or X–Se···Br fragments.

The data in Figure 1 (and in Figures S1-S6 in the ESI) also reveals the wide distribution of the X···Ch···Hal angles. While variations of the X···Ch···Hal angles are essentially continuous, especially at larger separations, two dominant values of these characteristics are noticeable in each distribution. Specifically, the X···Ch···Hal angles in the Te···I series are clustered around 180 ° and 110 °, and in the Se···Br series, the points are observed mostly around 180° and 90°. The linear geometry seems more favorable, especially in the Se···Br series. Such linear X···Ch···Hal arrangements facilitate hypervalent interactions, or, generally speaking, 3-center 4-electron (3c-4e) bonding, which might provide a bridge between covalent bonds and non-covalent interactions.[16] Thus, Ch···Hal contacts which are part of linear X···Ch···Hal fragments were considered as linear ones. Distributions of the linear and non-linear Ch···Hal contacts are illustrated in Figure 2.

Furthermore, considerations of the non-covalent interactions were focused on the line-of-site (LoS) contacts.[33] Such contacts are almost free from "shielded" effects of the neighboring atoms or groups and therefore they depend on the intrinsic properties of the interacting atoms. As such, the van der Waals radii (R_{Br} = 2.00 Å, R_I = 2.17 Å, R_{Se} = 2.04 Å) obtained earlier using LoS approach were used for the analysis in this study. Since similar radius for tellurium was not reported, its value, R_{Te} = 2.24 Å, was determined in this work (see *Methods* section).

A closer look at the linear X···Ch···Hal contacts reveals substantial variations in the distance distributions with the nature of the I–Te···I fragments are clustered mainly in the 2.7 Å – 3.0 Å range, and C–Te···I contacts are observed mostly in the 3.6 Å – 4.0 Å range, which could be roughly designated as essentially covalent and non-covalent regions.† Besides, some of these fragments populate the interim region, and I–Te···I lies in the lower part (3.0–3.4 Å), whereas C–Te···I lies in the upper part (3.4–3.6 Å). Apparently, the charge is distributed more or less equally between the iodine atoms in the symmetric I···Te···I fragments, and the corresponding bond lengths lie in the covalent region. On the contrary, the charge is concentrated on the iodine atom in the C–Te···I fragments, and the corresponding Te···I interactions represent the non-covalent chalcogen bond.[#] Substitution of carbon and iodine atoms in X–Te···I fragment by other elements, e.g., sulfur and selenium, results in higher probability of the formation of a fragment belonging to this intermediate region of the Te···I continuum (Figure 2c).

Almost all Te-centered non-covalent interactions are linear, and owing to the amphoteric (Lewis acid/base) nature of tellurium and iodine atoms, they correspond to halogen or chalcogen bonds. The most probable distance of the linear non-covalent Te···I interactions, denoted further as $D_{max}(Te\cdots I)^{spec}$, is estimated as 3.75 Å (Figure 3). This value is significantly lower than the sum of the van der Waals radii: $R_{Te} + R_I$ = 4.41 Å. These observations indicate the significant energy of Te···I chalcogen and halogen bondings.

The distance distribution of Se···Br contacts is analogous to that for the Te···I ones. It also can be divided into covalent (2.4–2.9 Å), interim (2.9–3.3 Å), and non-covalent regions (3.3–4.0 Å) (Figure 2d). The largest numbers of these contacts represent Br–Se···Br and

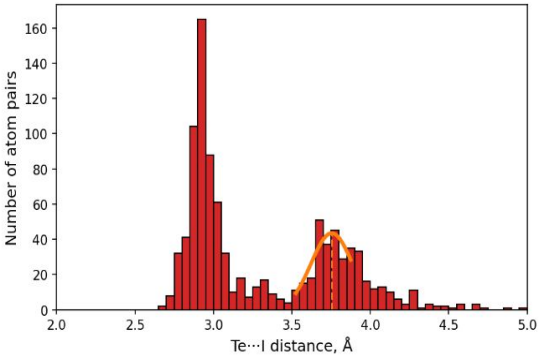

Figure 3. Distance distribution of the Te···I contacts, which are part of the linear X–Te···I fragments. Orange curve indicates van der Waals peak which is described by a probability density function of the normal distribution, and the dotted orange line shows its maximum $D_{max}(Te\cdots I)^{spec}$.

C–Se···Br fragments which are observed mainly in the covalent and the non-covalent regions, respectively (Figure 2e). The most probable distance of the linear non-covalent Se···Br interactions $D_{max}(Se\cdots Br)^{spec}$ = 3.57 Å (Figure 4) is also significantly lower than the sum of the corresponding van der Waals radii: $R_{Se} + R_{Br}$ = 4.04 Å.

Similar to the X–Te···I interactions, a significant fraction of X–Se···Br fragments with X = N, P, S, and Se belongs to the interim region (Figure 2f). However, there are two major differences between Se- and Te-containing contacts. First, there is a much higher fraction of non-linear non-covalent Se···Br interactions as compared to Te···I analogues (Figure 2d). The smaller number of Te···I intermediate structures is explained by the low fraction of "non-conventional" systems with X–Te···I fragments, where X is not C or I. Second, a dispersion of the distances of non-covalent Se···Br interactions is much higher than that for Te···I ones: 3.2–4.0 Å vs 3.5–4.1 Å. Both these observations suggest lower stabilization energy of hypervalent X–Se···Br interactions as compared to X–Te···I ones.

Overall, the analysis of the structural data confirms the existence of continuums of both Se···Br and Te···I interactions between covalent and non-covalent bonds. To examine changes of the nature of bonding with the interatomic distances, we carried out QTAIM analysis of the topological characteristics of electron densities and energies at BCPs along Ch···Hal bond paths in these systems.

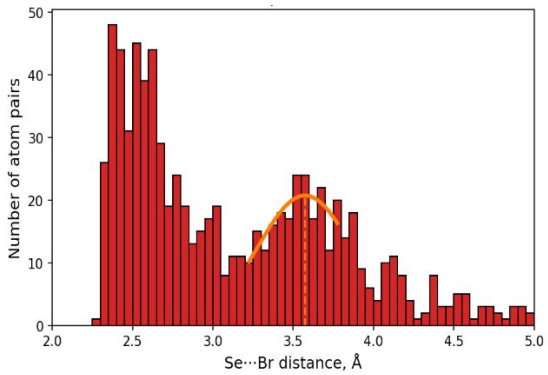

Figure 4. Distance distribution of the Se···Br contacts, which are part of the linear X–Se···Br fragments. Orange curve indicates van der Waals peak which is described by a probability density function of the normal distribution, and the dotted orange line shows its maximum $D_{max}(Se\cdots Br)^{spec}$.

2. QTAIM analysis of the Se···Br and Te···I interactions.

In order to evaluate variations of the characteristics of the BCPs on the interatomic distances, 21 structures with 50 non-equivalent Se-Br contacts were chosen (see Methods) from the Se-Br dataset to cover roughly uniformly a range from about 2.2 Å to 3.9 Å, i.e. from covalent Se-Br bond to the sum of the van der Waals radii of these atoms. These structures are shown in Figure S7 in the ESI.‡ In a similar way, 21 structures with 39 non-equivalent Te···I contacts covering a range from about 2.6 Å to 4.2 Å were chosen from the corresponding Te-I dataset (Figure S8 in the ESI). Since this study is focused on the chalcogen bonding, associations which were formed via Br···Se or I···Te halogen bonding were not included in these series.

Many of the structures under study represent chalcogen-bonded dimers illustrated in Figure 5 together with the BCPs obtained from the QTAIM analysis of these systems. These dimers show distinct (shorter and longer) Se···Br or Te···I separations. As such, topological characteristics of electron density and energy at BCPs of all these non-equivalent bonds were established and included in the analysis of the variations of their values with interatomic separations. The CSD refcodes of the representative structures and the crystallographically independent Se···Br and Te···I separations selected for the analysis are listed in Tables S1 and S2 in the ESI.

It should be noted that some of the structures under study represent fragments of the solid-state oligo- or polymeric associations. As such, their molecular geometries (and ChB characteristics) can be affected by the interatomic interactions with the extraneous parts, as well as by the crystal forces. To eliminate effects of the external interactions, the properties of BCPs at chalcogen bond paths were also established for the structures which were obtained by optimization of the selected fragments via DFT M062X/def2tzvpp computations.[39] Since the earlier studies showed that moderately-polar solvents represent optimal medium for the modelling of polar or ionic solid-state associations,[10] these optimizations were performed in vacuum and in dichloromethane. Calculated interatomic Se···Br and Te···I separations are listed together with the corresponding experimental values in Tables S1 and S2 in the ESI.

The relationships between experimental and calculated values for the Se···Br and Te···I systems are illustrated in Figure 6. The mean (signed) deviations of experimental values from the calculated ones are -0.08 Å and 0.02 Å for Se/Br systems and -0.13 Å and -0.06 Å for Te/I systems produced by calculations in vacuum and in dichloromethane, respectively. These data show that calculations, especially those with CH_2Cl_2 as a medium, reproduced experimental distances in chalcogen-bonded associations reasonably well. This confirmed that the calculated structures (which are free of the effects of crystal forces and extraneous interactions) represent reliable models which complement experimental associations in the QTAIM analysis of the

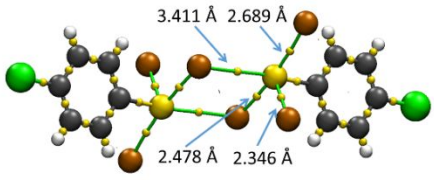

Figure 5. Bond paths (green lines) and BCPs (small yellow spheres) produced by the QTAIM analysis of the chalcogen-bonded 1-chloro-4-(tribromo-λ⁴-selanyl)benzene dimer (using coordinates extracted from ECIYIA)

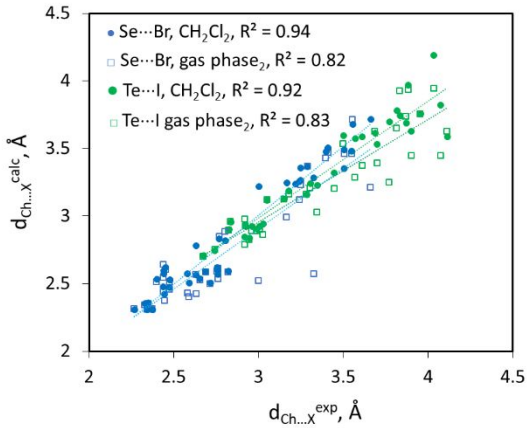

Figure 6. Correlations between experimental and calculated interatomic separations Se-Br (blue) and Te-I (green) (filled and open symbols represent values from calculations in dichloromethane and in vacuum, respectively).

chalcogen bonding**.** Most importantly, similarly to the solid-state structures, the calculated interatomic separations in the series of optimized complexes cover a whole range of values from covalent bonds to van der Waals separations. This affirms that such continuums represent the intrinsic property of ChB systems and is not a result of external factors.

Following the earlier QTAIM studies of the HB and HaB associations,[27-32] we focused our analysis on electron densities, ρ(r), the Laplacians, $\nabla^2\rho(r)$, kinetic and potential energy densities G(r) and V(r), and energy density H(r)= G(r) + V(r). These characteristics evaluated in the solid-state and optimized structures at the BCPs along the Se···Br and Te···I bond paths are listed in Tables S3 – S6 in the ESI.

The dependencies of the electron densities at BCPs on the interatomic Se···Br and Te···I separations are illustrated in Figure 7. Similar to the trends observed for HB and HaB complexes, the electron densities at chalcogen bonds' BCPs increase exponentially with the decrease of the interatomic Se···Br and Te···I separations. The points

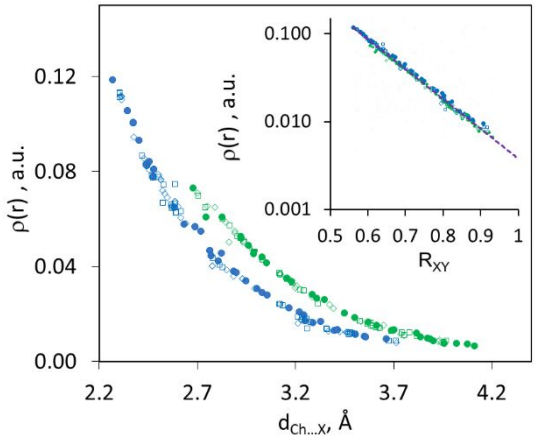

Figure 7. Dependencies of electron densities, ρ(r), at BCPs on the Se···Br and Te···I bond paths on the interatomic separations in associations extracted from the X-ray structures and in optimized complexes. Blue and green symbols show data for Se···Br and Te···I, respectively. Filled circles show characteristics determined in the experimental structures, and open squares and rhombics – data for the structures resulted from the optimizations in the gas phase and CH_2Cl_2, respectively (note that the same legend are used in all subsequent figures). Insert: Dependencies of ρ(r) (logarithmic scale) on the normalized interatomic separations. A violet dashed line shows the trend line for all data.

determined for the experimental and optimized structures follow the same trend lines for both Se···Br and Te···I systems. If the log ρ(r) values are plotted against normalized interatomic separations, R_{XY}, all points follow the same linear trend line with R^2 of 0.996. In a recent publication, a unified trend line was also found for the HaB complexes of bromosubstituted electrophiles with Cl^-, Br^- or DABCO.[31] Markedly, the trend line established earlier for the dependence of ρ(r) on the normalized HaB bond length for various halogen bonds is very close to that obtained for the Se···Br and Te···I bonds. This unified trend line indicates that the normalized bond length is a principal parameter which determines electron densities at BCPs for both halogen and chalcogen bond paths. It should be stressed that the exponential increase of ρ(r) with $d_{Ch...X}$ is related primarily to the corresponding variations of the electron densities of the free atoms. In fact, the ρ(r) vs $d_{Ch...X}$ dependence for the promolecules (constructed by the superposition of the non-interacting fragments extracted from the experimental structures containing Se···Br contacts) is close to that for the bonded systems (Figure 8, note that the ρ(r) values for the latter are somewhat higher at shorted separations due to concentration of electron density at BCPs between Se and Br in the bonded systems). Most important for the current work, however, is the existence of the uninterrupted and smooth continuity of the interatomic distances and bonding characteristics in ChB systems from the weak van der Waals interactions to the fully-developed covalent bonds.

The data in Figure 7 shows that the electron densities at BCPs for chalcogen bonds which are close to the van der Waals separations are about 0.01 a.u., which is typical for the closed-shell interactions such as ionic bonds and weak supramolecular bonds.[27-30] As interatomic distances decrease, the densities are increasing to about 0.1 a.u., which is typical for shared-shell interactions at R_{XY} near 0.6. To examine transitions between these limiting cases, we carried out an analysis of the Laplacians of electron density, $\nabla^2\rho(r)$, and energy densities at the Se···Br and Te···I BCPs.

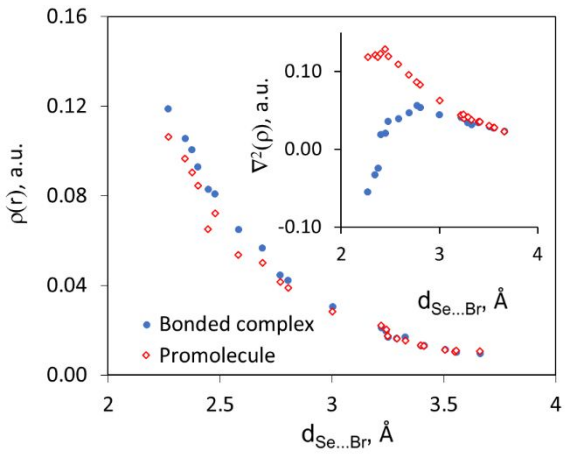

Figure 8. Variations of electron densities, ρ(r), at BCP along Se-Br bonds in the experimental structures (bonded complexes) containing Se-Br contacts and in the corresponding promolecules constructed by the superposition of the non-interacting fragments extracted from these experimental structures. Insert: Variation of the corresponding Laplacians of electron densities in the experimental (bonded) structures and promolecules.

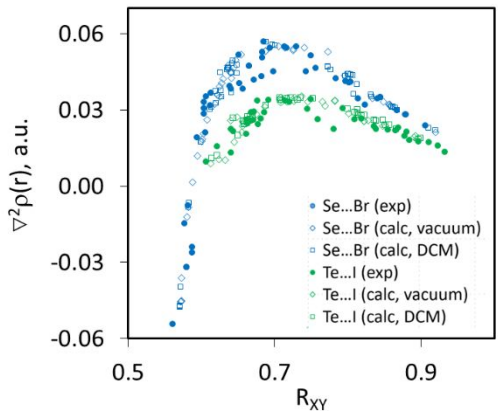

Figure 9. Dependencies of the Laplacians of the electron densities at BCPs on the Se···Br and Te···I bond paths (as indicated) on the interatomic separations.

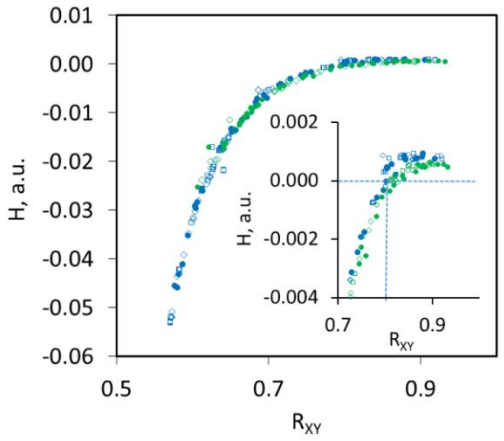

Figure 10. Dependence of energy density H(r) at BCPs on the Se···Br (blue) and Te···I (green) bond paths on the normalized interatomic separations. Inset: enlarged segment showing a transition from positive to negative values.

The variations of the values of $\nabla^2\rho(r)$ with the normalized Se···Br and Te···I separations are illustrated in Figure 9. In both series, the values of $\nabla^2\rho(r)$ follow similarly shaped curves analogous to that which were observed earlier in HB and HaB systems. At the Br···Y separations close to the sum of the van der Waals radii (i.e. R_{XY}~ 1), the Laplacians are positive and rather small. As the $d_{X\cdots Y}$ distance decreases, the $\nabla^2\rho(r)$ values are increasing, reach maxima at R_{XY} about 0.75 - 0.80 and then start to decrease. At comparable R_{XY} values, the magnitude of the Laplacians in the Se···Br systems is larger than those determined for the Te···I bonds. Besides, at the $d_{X\cdots Y}$ distances corresponding to the covalent bonds, the $\nabla^2\rho(r)$ values for the Se···Br bonds are negative, while those for the Te···I bonds remain positive. In comparison, analysis of the promolecules reveal no substantial decrease of $\nabla^2\rho(r)$ values at shorter separations (insert in Figure 8). Similar small positive or negative Laplacian values were found earlier for the other covalent bonds formed by highly polar atoms,[27,40-42] as well as in the HaB complexes.[31] This further confirms that in many cases, the negative values of Laplacians of electron densities are not a prerequisite of the covalent character of bonding. Therefore, if taken separately, they not a reliable indicator of the nature of bonding.

Energy densities, H(r), at the BCPs represent another characteristic which is commonly used for identification of the nature of interatomic interaction. The values of H(r) are determined by the relative magnitudes of the positive kinetic energy and negative potential energy densities, G(r) and V(r), respectively.[27] The variations of these characteristics in the Se···Br and Te···I series are shown in Figure S9 and their comparison with the corresponding characteristics of promolecules is illustrated in Figure S12 in the ESI. The kinetic energy density G(r) increases exponentially with a decrease of the interatomic separations $d_{X\cdots Y}$, and the points followed essentially the same curve for the Se···Br and Te···I series calculated using experimental and optimized coordinates. The magnitudes of the (negative) potential energy densities, V(r), are also increasing exponentially with the decrease of the interatomic separations. At large separations, the magnitudes of G(r) are higher than that of V(r), and therefore, the values of energy densities H(r) are positive (Figure 10). The changes of the values of V(r) with interatomic distances, however, are steeper than those of G(r), and potential energy dominates at shorter interatomic distances. As such, the total energy values of H(r) are negative and their magnitudes are increasing with the decrease of R_{XY}.

The dependencies of the H(r) on the normalized interatomic separations follow nearly the same curves for both Se/Br and Te/I systems (Figure 10). A closer look at the transitional region (shown as an insert in Figure 10) reveals that the energy densities at the BCPs along Te···I pathways are somewhat lower at large separations than that found for the BCPs for the Se···Br systems. Yet, the transition between positive and negative values of H(r) occurs in the Te···I series and in the Se···Br series at similar R_{XY} of about 0.80. A passage from the positive to negative values of H(r) was used previously as an indication of the changeover from non-covalent interactions to partially-covalent interactions.[27] It is, thus, important to note, that such transitions occur in the chalcogen-bonded systems under study at R_{XY} ~0.80, which is similar to that (0.75-0.80) found earlier in the halogen-bonded systems. This indicates that significant molecular orbital interactions in chalcogen-bonded pairs occur at about the same distances as that in the HaB associations. As R_{XY} values decrease to about 0.65 or less, the electron densities approach 0.1 a.u. value. When the $\nabla^2\rho(r)$ values are close to zero or negative and H(r) values are negative, and magnitudes of the negative values of H(r) is increasing sharply with the decrease of R_{XY}. These features indicate the essentially covalent character of Se- and Te-involved interactions in this range. This data also supports the suggestion that normalized interatomic distances can be used as a basic parameter determining nature (non-covalent, partially covalent or non-covalent) of the interaction.

Methods.

Version 5.42 (November 2020) of CSD[25] was used for the selection of crystals for the subsequent analysis. Disordered, erroneous, polymeric, pressurized, powder structures and experiments with R-factor > 0.1 were removed from consideration. Each polymorph was represented with one entry with the lowest R-factor value. Filtering of line-of-sight contacts[33] was carried out using the filter_los_csd utility.[38] C–H, N–H, and O–H bond lengths were normalized to CCDC/ConQuest defaults: C–H 1.089 Å, N–H 1.015 Å, O–H 0.993 Å. Entries with the crystallographic cell volume exceeding 10 000 Å^3 were ignored (less than 5% of entries).

Following the earlier publication, the van der Waals radius of Te was determined as the weighted average of the difference between

the most probable distance of C–H···Te and C_{sp2}···Te line-of-sight contacts (Figures S10 and S11 in the ESI) and H_C (1.21 Å) and C_{sp2} (1.87 Å) line-of-sight van der Waals radii, respecttively.[38] Numbers of contacts shorter than the most probable distance were used as weighting coefficients. Te atoms forming more than four covalent bonds were not considered due to significant steric hindrance.

To analyze the continuum of Se–Br and Te–I interactions, data on covalent Ch–Hal bonds and line-of-sight Ch···Hal contacts were extracted from CSD and combined into one dataset. Each Ch–Hal interaction was classified as common or linear based on whether Hal atom is part of linear X–Ch–Hal fragment, which is typical for hypervalent systems and linear chalcogen bonds.[43] X–Ch–Hal fragments were considered as linear if the X–Ch–Hal angle exceeds cutoff of 150 degrees, which is commonly used as linearity criterion for hydrogen bonds.[44] The resulting dataset was further used to plot and analyze distributions of distances of Ch –Hal interactions and to determine atomic radii of Se and Te in the linear chalcogen interactions.

21 structures with 50 non-equivalent Se-Br contacts and 21 structures with 39 non-equivalent Te···I contacts were chosen from the whole dataset for the QTAIM analysis. These structures are shown in Figures S7 and S8 in the Supporting Information. Among variety of different structures, about dozen of structures containing neutral or anionic aryl-Se···Br and aryl-Te···I fragments and close to linear X-Ch-Hal fragment were selected randomly to cover roughly uniformly a range the corresponding covalent Ch-Hal bond to the sum of the van der Waals radii of these atoms. Subsequently, several substances without aryl groups were added (e.g. dimethyl-((methyltelluro)ethynyl)telluronium iodide, bromodiselenocyanate, N,N-dimethylselenourea-dibromide, N1, N1, N3, N3-tetramethyl-a,a'-diselenobisformamidinium dibromide) to verify the independence of the results on the substituents of Ch atoms. The absence of the substantial scattering of points for Se/Br and Te/I series in Figures 6, 7, 9,10 and S9 confirmed that the normalized interatomic separations is a single most important parameter which determines characteristics under study, and the nature of substituents on chalcogen atom and/or charge of the complex have minor effect.

Quantum-mechanical calculations were carried out with the Gaussian 09 suite of programs.[45] Geometries of the ChB associations were optimized without constraints using DFT, M062X/6-311+G(d,p), calculations with the basis set.[39] Previous theoretical analyses indicated that it produces excellent geometries and energies of supramolecular complexes at a reasonable computational cost.[46,47] The coordinates extracted from the X-ray structures of these associations were used as the starting points in the optimizations. The absence of the imaginary vibrational frequencies confirmed that the optimized structures represented true minima. Calculations in dichloromethane were carried out using a Polarizable Continuum Model.[48] This moderately-polar solvent represents a good media for modelling solid-state ionic compounds. Energies and coordinates of all experimental and optimized structures are listed in the ESI.

The QTAIM analyses were carried out with the Multiwfn program.[49] The results were visualized using the molecular graphics program VMD.[50] The wfn output files for such analysis were produced with Gaussian 09 via single-point calculations of the experimental or optimized complexes

Conclusions

Combined CSD and QTAIM analyses revealed remarkable continuums of Ch-Hal distances, as well as topological characteristics of the electron densities and energies at BCPs along the Ch-Hal bond paths. At the limit of short separations, they were typical for the covalent bonds. At the limit of large separations, these characteristics were common for the closed-shell (non-covalent) interactions. As in the halogen-bonded systems, the characteristics of the chalcogen-containing associations varied synchronously when plotted against normalized interatomic separations, with the changeover from the essentially non-covalent to partially-covalent interactions occurring at normalized bond lengths $R_{XY} \approx 0.80$, and transition to essentially covalent bonding taking place at R_{XY} of about 0.65. These features confirm fundamental similarity of these bondings and support a suggestion that R_{XY} values represent a basic parameter determining the nature of bonding.

Together with the reported earlier analogous data in the HB and HaB systems, the results of the current work confirm a general character of a covalent-to-supramolecular bonding continuums regardless of the type of bonding. Most importantly, uninterrupted continuums of bond distances from van der Waals separations to the fully developed covalent bonds together with continuous and smooth dependencies of all topological characteristics of the electron density and energy demonstrated an intrinsic link between limiting (covalent and supramolecular) types of bondings.[‡]

Author Contributions

D.K.M – Optimization and QTAIM analysis of the ChB complexes, writing- review and editing, I.Yu.C. – CSD analysis, visualization, writing- review and editing, Yu.V.T. conceptualization, CSD analysis, writing – original draft, review and editing, S.V.R.: conceptualization, funding acquisition, data curation, visualization, writing – original draft, review and editing

Conflicts of interest

There are no conflicts to declare.

Acknowledgements

D.K.M and S.V.R thank the National Science Foundation (grant CHE-2003603) for financial support of this work. Calculations were done on Ball State University's beowulf cluster, which is supported by The National Science Foundation (MRI-1726017) and Ball State University. Y.T. thanks the Russian Scientific Foundation (grant № 19-13-00338) for the financial support and shared experimental facilities supported by Kurnakov Institute of General and Inorganic Chemistry RAS for CSD access.

Notes and references

$ The definitions of ChB and HaB shares the same issue of using the kinetic electrophilic/nucleophilic terms to define a thermodynamic concept. This issue (along with the use of the yet formally, undefined by IUPAC at that momentphicogen and tetrel bonding in the further description of ChB) requires a separate consideration and it is not a focus of the current work. Yet, it is mentioned to point out the other, a general issue of all definitions: in attempt to separate some phenomenon out of the complex background, the complexity and continuity of the background is commonly missed.

† The term "non-covalent" is commonly used (including current work) to identify HaB and ChB bonds, (e.g. definition of the latter states "…the term "chalcogen bond" is used uniquely to designate the latter set of noncovalent interactions described above"[6]). Yet, the experimental and computational data indicate that even though their energy is usually far less than that for the weakest bond one can consider as genuinely covalent, these "noncovalent" interactions may have certain degree of covalency. The continuum from the covalent to noncovalent interactions presented in the current work can be considered as a seamless increase (decrease) of the covalent contribution in ChB interactions.

$$ For comparison, please see the CSD scatterplots for Te-O, Te-Cl, Te-Br, Se-Cl and Se-I geometry (which are generally similar to those involving Te-I and Se-Br pairs) in Figures S3-S6 in the ESI. Also, while the QTAIM analysis in the current work was based on the computational data, there are a number of publications which report experimental high resolution charge-density analyses of ChB systems.[51-53] Yet, the experimental data allowing to examine continuums from weak interactions to covalent bond are not available. Also, earlier thorough analysis[51] demonstrated good agreement between experimental and theoretical characteristic (ρ, $\nabla^2\rho(r)$, G, V) of ChB associations, which support the validity of the computational approach.

#This can be explained by the somewhat higher electronegativity of iodine as compared to carbon atoms. Indeed, in hypervalent 3c-4e X···Ch···Y interactions the "excessive" electron pair is distributed between X and Y depending on their electronegativity: the higher the electronegativity, the higher the electron density on the corresponding atom, and the longer the corresponding bond.

‡Alternative hypothesis (that variation cannot be continuous) implies a switch from one type of distinct bonding to another at some point with corresponding abrupt changes in the bonding characteristic which is at variance with the data reported herein.

1. G. Cavallo, P. Metrangolo, R. Milani, T. Pilati, A. Priimagi, G. Resnati and G. Terraneo, *Chem. Rev.,* 2016, **116**, 2478.
2. L. Gilday, S. Robinson, T. Barendt, M. Langton, B. Mullaney and P. Beer, *Chem. Rev.,* 2015, **115**, 7118.
3. L. Vogel, P. Wonner and S. Huber, *Angew. Chem. Int. Ed.* 2019, **58**, 1880.
4. S. Scheiner, Acc. *Chem. Res.,* 2013, **46**, 280.
5. A. Bauzá, T. Mooibroek and A. Frontera, *Angew. Chem. Int. Ed.,* 2013, **52**, 12317.
6. G. Desiraju, P. Ho, L. Kloo, A Legon, R. Marquardt, P. Metrangolo, P. Politzer, G. Resnati and K. Rissanen, *Pure Appl. Chem.,* 2013, **85**, 1711.
7. C. Aakeroy, D. Bryce, G. Desiraju, A. Frontera, A. Legon, F. Nicotra, K. Rissanen, S. Scheiner, G. Terraneo, P. Metrangolo and G. Resnati, *Pure Appl. Chem.,* 2019, **91**, 1889.
8. Y. Torubaev, F. Dolgushin, I. Skabitsky, and A. Popova, *New J. Chem*, 2019, **43**, 12225.
9. C. Weinberger, R. Hines, M. Zeller and S. Rosokha, *Chem. Commun.,* 2018, **54**, 80603
10. C. Loy, M. Zeller and S. Rosokha, *Crystals*, 2020, **10**, 1075.
11. V. Oliveira and D. Cremer, *Chem. Phys. Letters,* 2017, **681**, 56.
12. K. Donald and M. Tawfik, *J. Phys. Chem. A*, 2013, **117**, 14176.
13. N. Liu, X. Xie, Q. Li and S. Scheiner, *Chemphyschem*, 2021.
14. (a) V. Oliveira, E. Kraka and D. Cremer, *Phys Chem Chem Phys,* 2016, **18**, 33031. (b) S. Yannacone, V. Oliveira, N. Verma and E. Kraka, *Inorganics*, 2019, **7**, 47.
15. M. Aragoni, M. Arca, F. Devillanova, A. Garau, F. Isaia, V. Lippolis and A. Mancini, *Bioinorg. Chem. Appl.,* 2007, 17416.
16. M. Aragoni, M. Arca, F. Devillanova, F. Isaia, V. Lippolis, *Cryst. Growth Design*, 2012, **12**, 2769.
17. S. Alvarez, *Dalton Trans*., 2013, **42,** 8617.
18. T. Chivers and R. Laitinen, *Chem Soc Rev.*, 2015, **44**, 1725.
19. A. Cozzolino, P. Elder and I. Vargas-Baca*, Coord. Chem. Revs.*, 2011, **255**, 1426.
20. L. Wolters and M. Bickelhaupt, *ChemistryOpen,* 2012*,* **1***,* 96.
21. L. Santos, S. Lubbe, A. Hamlin, C. Ramalho and F. Bickelhaupt, *ChemistryOpen*, 2021, **10**, 391.
22. O. Grounds, M. Zeller and S.V. Rosokha, *New J. Chem.*, 2018, **42**, 10572.
23. V. Angarov and S. Kozuch, *New J. Chem.*, 2018, **42**, 1413.
24. C. Groom, I. Bruno, M Lightfoot and S. Ward, *Acta Cryst. Section B: Struct. Sci. Cryst.Eng. Mater.*, 2016, **72,** 171.
25. Cambridge Structural Database (CSD), Version 5.42 (Nov. 2020), Cambridge Crystallographic Data Centre, UK.
26. R. Bader, *Chem. Rev,* 1991, **91**, 893.
27. P. Popelier, *The QTAIM perspective of chemical bonding in The Chemical Bond*, John Wiley & Sons, Ltd, 2014, 271.
28. I. Mata, I. Alkorta, E. Espinosa and E. Molins, *Topological properties of the electron distribution in hydrogen-bonded systems.* In *The quantum theory of atoms in molecules.* C. Matta and R Boyd, Eds. Wiley-VCH Verlag Weinheim 2007, 425
29. E. Espinosa, I. Alkorta, J. Elguero and E. Molins, *J. Chem. Phys.* 2002, **117**, 5529.
30. P. Mallinson, G. Smith, C, Wilson, E. Grech and J. Wozniak, *Am. Chem. Soc.*, 2003, **125**, 4259.
31. D. Miller, C. Loy and S. Rosokha, *ACS Omega*, 2021, **6**, 23588.
32. S. Grabowski, *J. Phys. Chem. A,* 2012, **116**, 1838.
33. R. Taylor, *CrystEngComm,* 2014, **16**, 6852.
34. A. Bondi, *J. Phys. Chem.*, 1964, **68***,* 441.
35. M. Mantina, A. Chamberlin, R. Valero, C. Cramer and D. Truhlar, *J. Phys. Chem. A,* 2009, **113**, 5806.
36. P. Politzer and J. Murray, *Struct. Chem.,* 2021, **32**, 623.
37. M. Rahm, R. Hoffmann and N. Ashcroft, *Chem. Eur. J.,* 2016, **22**, 14625.
38. I. Chernyshov, I. Ananyev and E. Pidko, *Chemphyschem*, 2020, **21**, 370.
39. Y. Zhao and D. Truhlar, *Theor. Chem. Acc.,* 2008, **120**, 215.
40. Cremer, D.; Kraka, E. A *Croatica Chem. Acta,* **1985**, 57, 1259.
41. G. Gibbs, D. Cox, T. Crawford, K. Rosso, N. Ross and R. Downs, *J. Chem. Phys.* 2006, **124**, 084704.
42. G. Gervasio, R. Bianchi and D. Marabello, *Chem. Phys. Letters* 2004, **387**, 481.
43. K. Mahmudov, M. Kopylovich, M. da Silva, A. Pombeiro, *Dalton Trans,* 2017, **46**, 10121.

44. I. Chernyshov, M. Vener, P. Prikhodchenko, A. Medvedev, O. Lev and A. Churakov, *Cryst. Growth Design*, 2016, **17**, 214.
45. M. Frisch, G. Trucks, H. Schlegel, G. Scuseria, M. Robb, J. Cheeseman, G. Scalmani, V. Barone, B. Mennucci, G. Petersson, H. Nakatsuji, M. Caricato, X. Li, H. Hratchian, A. Izmaylov, J. Bloino, G. Zheng, J. Sonnenberg, M. Hada, M. Ehara, K. Toyota, R. Fukuda, J. Hasegawa, M. Ishida, T. Nakajima, Y. Honda, O. Kitao, H. Nakai, T. Vreven, J. Montgomery, Jr., J. Peralta, F. Ogliaro, M. Bearpark, J. Heyd, E. Brothers, K. Kudin, V. Staroverov, R. Kobayashi, J. Normand, K. Raghavachari, A. Rendell, J. Burant, S. Iyengar, J. Tomasi, M. Cossi, N. Rega, J. Millam, M. Klene, J. Knox, J. Cross, V. Bakken, C. Adamo, J. Jaramillo, R. Gomperts, R. Stratmann, O. Yazyev, A. Austin, R. Cammi, C. Pomelli, J. Ochterski, R. Martin, K. Morokuma, V. Zakrzewski, G. Voth, P. Salvador, J. Dannenberg, S. Dapprich, A. Daniels, O. Farkas, J. Foresman, J. Ortiz, J. Cioslowski, and D. Fox, *Gaussian 09, Rev. C.01,* Gaussian, Inc., Wallingford CT, 2009.
46. A. Bauzá, I. Alkorta, A. Frontera and J. Elguero, *Chem. Theory Comput.,* 2013, **9**, 5201.
47. Z. Zhu, Z. Xu, and W. Zhu, *J. Chem. Inf. Model*., 2020, **60**, 2683.
48. J. Tomasi, B. Mennucci, and R. Cammi, *Chem. Rev.,* 2005, **105**, 2999.
49. T. Lu, and F. Chen, *Comput. Chem.,* 2012, **33**, 580.
50. W. Humphrey, A. Dalke and K. Schulten, *J. Mol. Graphics* 1996, **14**, 33.
51. M. E. Brezgunova, J. Lieffrig, E. Aubert, S. Dahaoui, P. Fertey, S. Lebègue, J. G. Ángyán, M. Fourmigué and E. Espinosa, *Cryst. Growth Design*, 2013, **13**, 3283.
52. M. Pyziak, J. Pyziak, M. Hoffmann and M. Kubicki, *Cryst. Growth Design*, 2015, **15**, 5223.
53. S. P. Thomas, D. Jayatilaka and T. N. G. Row, *Phys. Chem. Chem. Phys.*, 2015, **17**, 25411.